KSCE Journal of Civil Engineering (2020) 24(8):2304-2321
DOI 10.1007/s12205-020-1386-2

pISSN 1226-7988, eISSN 1976-3808
www.springer.com/12205

Geotechnical Engineering

Experimental Study on the Mechanical Behaviour of Natural Loess Based on Suction-Controlled True Triaxial Tests

Fang Zheng[a], **Shengjun Shao**[a], **Jiao Wang**[a], **and Shuai Shao**[a]

[a]*Dept. of Civil and Architecture Engineering, Xi'an University of Technology, Xi'an 710048, China*

ARTICLE HISTORY

Received 14 August 2019
Revised 2 March 2020
Accepted 21 April 2020
Published Online 30 June 2020

KEYWORDS

Natural loess
Matric suction
True triaxial apparatus
Stress-strain response
Failure envelopes

ABSTRACT

Loess is mostly distributed in an unsaturated state in nature, and the complexity of the engineering properties of unsaturated soil is mainly due to the existence of matric suction. Therefore, matric suction must be considered in investigating the mechanical properties of unsaturated loess. However, soils are most often subjected to three principal stresses with different magnitudes in practical engineering. For the sake of examining and discussing the mechanical behaviour of unsaturated natural loess under a complex stress path, a suction-controlled true triaxial apparatus with a rigid-flexible boundary is used to test unsaturated natural loess under a complicated stress path. Four trials of isotropic consolidation tests are conducted on natural loess under suction-controlled conditions via the true triaxial apparatus. The consolidation yield characteristics of the natural loess under different matric suctions are investigated. Forty-eight trials of consolidated drained true triaxial tests under suction-controlled conditions are conducted on unsaturated natural loess to examine and discuss the influence of the matric suction and intermediate principal stress parameter (*b*-value). The consolidated drained trials are performed under a constant net mean stress and a constant matric suction with different intermediate principal stress parameters (*b*-values). Stress-strain curves and failure envelopes of the natural loess are also presented. The results indicate that the stress-strain-strength response of unsaturated natural loess depends on the matric suction and intermediate principal stress parameter under true triaxial conditions.

1. Introduction

Loess, a Quaternary deposit in arid and semi-arid arid areas, has many internal material components and external morphological characteristics, which are different from other deposits from the same period and have certain regularities in geographical distribution. Loess is widely distributed in many parts of the world, such as America (Rogers et al., 1994; Zárate, 2013), Asia (Phien-Wej et al., 1992; Ryashchenko, 2008; Porter, 2013) and Europe (Rousseau et al., 2007), which accounts for one tenth of the Earth's land area (Zhang et al., 2018). Loess in China is famous for its wide distribution, high continuity, well-developed strata and great thickness (Sun, 2002; Liu et al., 2015). The Loess Plateau is the most representative region of loess distribution in China. The geological history of the Loess Plateau since the Quaternary Period allowed the loess to be continuously distributed across a large area, with considerable stratigraphic deposition and complete preservation, providing a natural test site in which to study loess.

Loess has special properties, such as a certain water sensitivity, macroporous structure and collapsibility (Li et al., 2016; Zhang et al., 2018; Xing et al., 2019). Many engineering problems, such as the uneven settlement of building foundations, wetting-induced landsliding of loess and the collapse of tunnels, are caused by these special properties in high-humidity areas (e.g., Tan, 1988; Derbyshire, 2001; Kim and Kang, 2013; Fan et al., 2017; Luo et al., 2018). Therefore, it is inevitable to explore and investigate the related mechanical properties of loess. Loess is a kind of typical unsaturated soil. For a long time, most research on the mechanical behaviour of loess was based on the general total stress method of soil mechanics. However, with the development of soil mechanics on unsaturated soil, research on the mechanical behaviour of unsaturated loess has attracted attention over the past few years. Studying the basic characteristics

CORRESPONDENCE Shengjun Shao sjshao@xaut.edu.cn Dept. of Civil and Architecture Engineering, Xi'an University of Technology, Xi'an 710048, China

of loess by using the strength-deformation theory of unsaturated soil has become popular.

Unsaturated soil is composed of three phases: liquid phase, solid phase and gas phase. The existence of the gas phase further complicates the mechanics character of the unsaturated soil. The matric suction (s) on the surface of these three phases is crucial in investigating unsaturated soils because it makes a notable influence on the mechanics character of unsaturated soil. Thus, research on the characteristics of matric suction ($s = u_a - u_w$) of unsaturated loess is still one of the most active and representative parameters in soil behaviour studies. Due to the complexity of the properties of unsaturated loess, it is very difficult to fully explore theoretically. It is necessary to determine the law governing the soil behaviour via experimental means and then perform a theoretical analysis. Although lots of experimental research has been performed to reveal loess behaviour, for example, studies based on oedometer tests (e.g., Jiang and Shen, 1998; Liu et al., 2015), direct shear tests (e.g., Matalucci et al., 1970; Sheng et al., 2010), and conventional triaxial tests (e.g., Jiang et al., 2014; Xing et al., 2016), some of them have also been performed with the consideration of the effect of matric suction on loess behaviour (e.g., Sheng et al., 2010; Chen et al., 2014; Gao et al., 2017; Ng et al., 2017). However, these experimental studies on unsaturated loess with regard to matric suction (s) are limited to a consolidometer, direct shear apparatuses and conventional triaxial apparatuses, and the stress paths that can be achieved are limited. For example, the intermediate (σ_2) and minor principal stresses (σ_3) are equal under conventional triaxial conditions. However, in practical engineering, the forces applied to soil often vary among the three orthogonal directions. To reflect the complex stress states of unsaturated soil more realistically, a true triaxial test must be conducted. Although a few experiments on unsaturated loess have been conducted via true triaxial testing (e.g., Shao et al., 2017), the effect of matric suction (s) on unsaturated loess has not been taken into account.

Hence, it is necessary to examine and discuss the soil behaviour of unsaturated loess by combining the intermediate principal stress parameter (b) with the matric suction (s). This work aims to investigate and discuss the strength characteristics of natural loess under a multiaxial stress state along different suction stress paths. Several isotropic consolidation tests on natural loess under different suction conditions are carried out to discuss the yield characteristics of undisturbed loess under mean stress. Several groups of true triaxial shear tests under suction-controlled conditions are performed on intact loess with different intermediate principal stress parameter values. In the experimental shearing process, the matric suction (s) is controlled to be constant while the net mean stress (p) is kept unchanged. The results are obtained to analyse the stress-strain-strength characteristics of natural loess under a complex stress state. There is little research on the properties of natural loess under suction-controlled true triaxial conditions. The lack of this type of experimental evidence for natural loess is the main motivation of this paper.

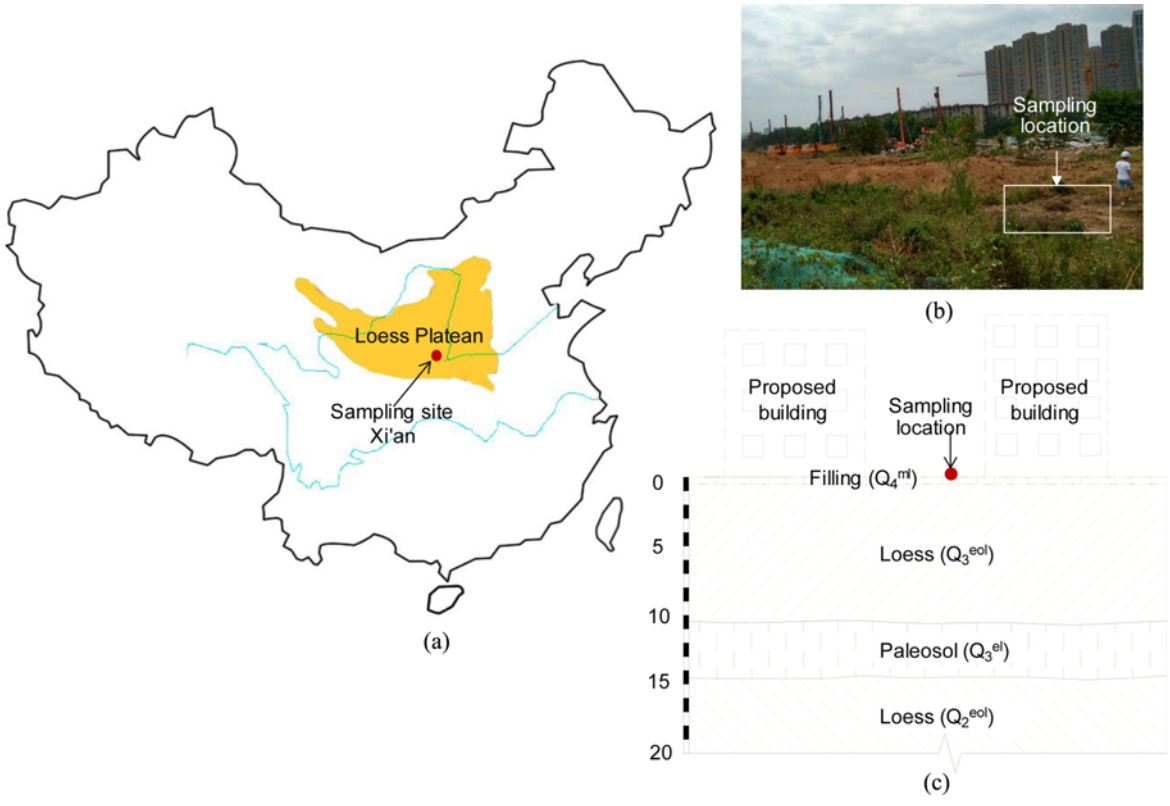

Fig. 1. Sampling Overview: (a) Location, (b) Photo of the Sampling Field, (c) Soil Profile

2. Characteristics of the Tested Soils and Specimen Preparation

2.1 Sampling Location

The tested loess was taken from a construction site in Xi'an city, Shaanxi Province, China (Figs. 1(a) – 1(b)). The undisturbed block samples were collected at a depth of 4.0 m – 5.0 m. After an exploratory well was dug manually, undisturbed samples with dimensions of 40 cm × 40 cm × 40 cm were collected. The soil profile is given in Fig. 1(c), indicating that the tested loess is Q3 loess.

2.2 Physical Characteristics of the Tested Loess

The basic physical indices of tested loess are given in Table 1. According to loess classification (Gibbs and Holland, 1960), the loess tested in this work is classified as silty loess (Fig. 2).

The particle size distribution curve of tested loess is presented in Fig. 3. The loess is mostly made of silty particles, with a proportion of 78%, and clay particles, with a proportion of 20.9%.

The soil-water characteristic curve (commonly referred to simply as the SWCC) of tested loess is presented in Fig. 4. The SWCC was obtained via a consolidation apparatus for unsaturated soil. The measurement range of the suction value is from 0 kPa to 450 kPa along the drying path. The SWCC model suggested by Van Genuchten (1980) was adopted to fit the experimental data.

Table 1. Basic Physical Indices of Tested Loess

Soil property	Value
Specific gravity, G_s	2.70
Natural moisture content, w/%	13.2 – 15.8
Natural dry density, ρ_d/g·cm^{-3}	1.30
Initial void ratio, e_o	1.08
Clay fraction/%	20.9
Silty fraction/%	78.0
Sand fraction/%	1.1
Atterberg limits	
Liquid limit, w_l/%	31.7
Plastic limit, w_p/%	20.6
Plasticity limit, I_p	11.1

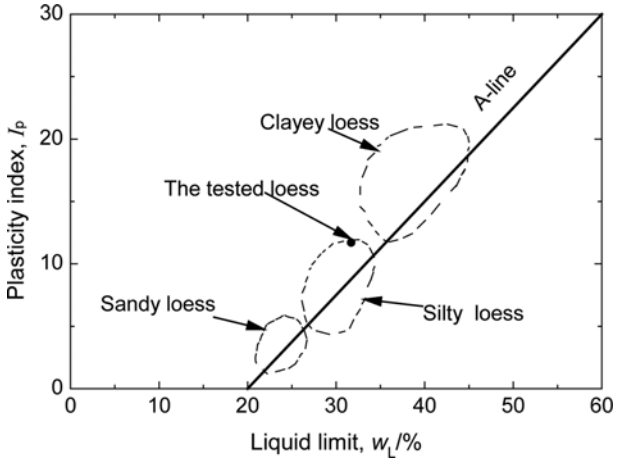

Fig. 2. Classification of Tested Loess (Gibbs and Holland, 1960)

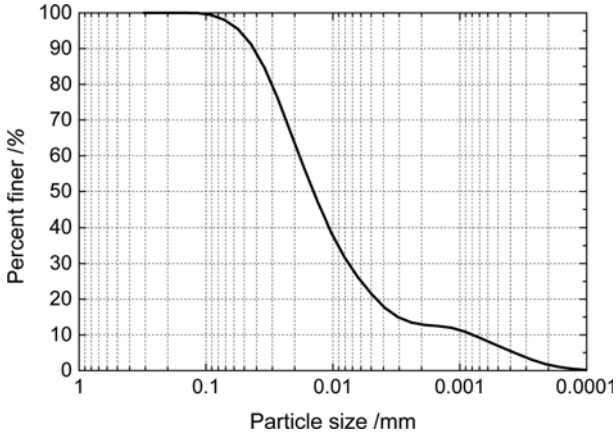

Fig. 3. Particle Size Distribution Curve of Tested Loess

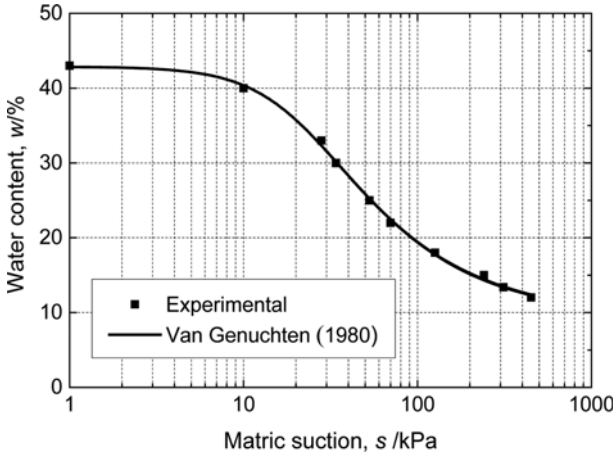

Fig. 4. Soil-Water Characteristic Curve of Tested Loess

2.3 Preparation of Specimens

For the samples used in the tests, soil blocks with an average dry density of 1.30 g/cm^3 are selected, and the density differences of samples are controlled to be within 0.03 g/cm^3 to reduce the influence of the dry density on the experimental results. The natural specimens (70 mm × 70 mm × 140 mm) are cut from the large soil blocks via a custom-made sample cutting apparatus.

To save time, before the experiment, the moisture contents (w) of the specimens corresponding to the different matric suctions (s) can be determined by using the SWCC of this natural loess. Then, the corresponding moisture contents of the specimens are prepared according to the experimental requirements. When specimens with a moisture content lower than that of the natural samples need to be prepared, the air-drying method is adopted. The samples are placed in a cool place to induce water evaporation. The weights of the samples are continuously measured until the required moisture content is reached. For the specimens with a

higher moisture content, the water membrane transfer method is used; that is, the dropper is titrated evenly across the specimen until the required moisture content is reached. According to experience, it is best to rest specimens for more than 96 h to ensure that the moisture can be dispersed evenly throughout the sample. The preparation of the saturated samples is carried out via a pumping saturation method. First, the samples are placed into the true triaxial saturator and are then exhausted of air in a vacuum cylinder for saturation. The specimens are pumped in an empty vacuum for 45 minutes, pumped for another 30 minutes after distilled water is added, and then submerged for 24 hours. Each of these specimens is covered by two pieces of filter paper and two water-permeable stones on the top and bottom to prevent any interference during the saturation process.

3. Test Apparatus

3.1 Experimental Principle

Matric suction (s) is expressed as $s = u_a = u_w$, where u_a and u_w indicate pore air pressure and pore water pressure, respectively. In general, the pore water pressure of unsaturated loess is always negative. There is much difficulty in measuring the value of negative pore water pressure (u_w), because the water may undergo cavitation when the water pressure approaches -100 kPa (Hoyos and Macari, 2001). Therefore, based on the principle of the axial translation technique, the value of pore water pressure (u_w) can be raised to a range convenient for measurement. After the pore water pressure (u_w) is increased artificially, the pore air pressure (u_a) is also increased at the same time, but the difference ($u_a - u_w$) remains unchanged; that is, the matric suction (s) remains unchanged. Thus, the matric suction (s) can be measured or controlled via the axial translation technique.

The realization of the axial translation technique depends on a ceramic disk with a high air intake value. The material of the ceramic disk with a high air intake value is permeated by water but not air within its limited intake value, and thus, the pore water pressure (u_w) is separated from pore the air pressure (u_a). This type of ceramic disk material has many uniform micro-pores. When the ceramic disk is completely saturated, the surface of the ceramic disk forms a contraction film, which allows water to permeate. The top surface of the ceramic disk bears pore air pressure, while the bottom surface bears pore water pressure; thus, the independent control and measurement of these two pressures can be conducted. In this experiment, this kind of ceramic disk with an intake value of 500 kPa is fastened to the pedestal of the apparatus. Furthermore, the pore water pressure is zero ($u_w = 0$), and thus, the matric suction is assumed to be equal to the pore air pressure ($s = u_a$), which is easy to measure and control.

Before the experiment, the ceramic disk is saturated by a method similar to that described in the saturated sample preparation section below.

3.2 Introduction of the True Triaxial Apparatus

True triaxial apparatuses can be divided into three types according to the loading boundary conditions: rigid boundary type (e.g., Hambly, 1969; Ibsen and Praastrup, 2002); flexible boundary type (e.g., Ko and Scott, 1967; Reddy et al., 1992; Choi et al., 2008); and rigid-flexible mixed boundary type (e.g., Kirkgard and Lade, 1993; Yin et al., 2010). However, there are few true triaxial devices that can control matric suction, such as the following two devices. Matsuoka et al. (2002) introduced a suction-controlled true triaxial device with rigid boundaries. Since the loading is applied by three rigid plates, the stress path that the device can achieve is limited. As the negative pore water pressure (i.e., $s = -u_w$) method is used to control the matric suction, the controlled matric suction is also limited. Hoyos et al. (2012) introduced a true triaxial device with flexible boundaries. This device can achieve a more complex stress path, and the suction it can control is higher than that for the device introduced by Matsuoka et al. (2002). However, its flexible boundaries may interfere with each other. A new suction-controlled true triaxial apparatus with a mixed rigid-flexible boundary is used in this experiment. The loading mode of the device includes the following components: a pair of rigid plates along the axial direction, which are used to realize the load along the major principal stress (σ_2) direction, and two pairs of flexible lateral boundaries, both of which are comprised of four hydraulic rubber bags, that are used to realize the lateral loads along the directions of the intermediate principal and the minor principal stresses (σ_2, σ_3). The size of the specimens is 70 mm × 70 mm × 140 mm. The soil specimens are enclosed in a custom-built rubber membrane. Each soil specimen is fixed between pressure chambers, a rigid pedestal and a rigid loading cap. The four hydraulic rubber bags are sealed in the four pressure cells. The ceramic disk with a high intake value is fixed to the pedestal via screws, and the porous plastic disk is installed on the top of the specimens.

Figure 5 presents a detailed schematic of the main components of the device, including the pressure chamber, water/air control system and hydraulic drive system. Forces are imposed on specimens in three directions via three independent servo-driven systems. The servo stepping motor drives the roller screw to push the hydraulic cylinder piston to generate the hydraulic source, which is respectively connected with the vertical piston at the axial bottom of the pressure chamber and the lateral hydraulic rubber bags. Then, through the hydraulic transducer and displacement transducer, the independent loading and independent parameter measurements in three directions are realized, respectively. Pressure cylinder 1 is filled with hydraulic fluid to conduct stress application along the vertical direction. Both cylinders 2 and 3 are filled with distilled water, and the cylinders are connected to the four hydraulic rubber bags to apply lateral pressures. Pore air pressure (u_a) is provided by an external air compressor entering through the plastic porous plastic disk on the top of specimens. A ceramic disk is fixed on the pedestal via screws before the specimen is installed, which has a high air entry value of 500 kPa, thus the pore air pressure (u_a) is separated from the pore water pressure (u_w) during testing.

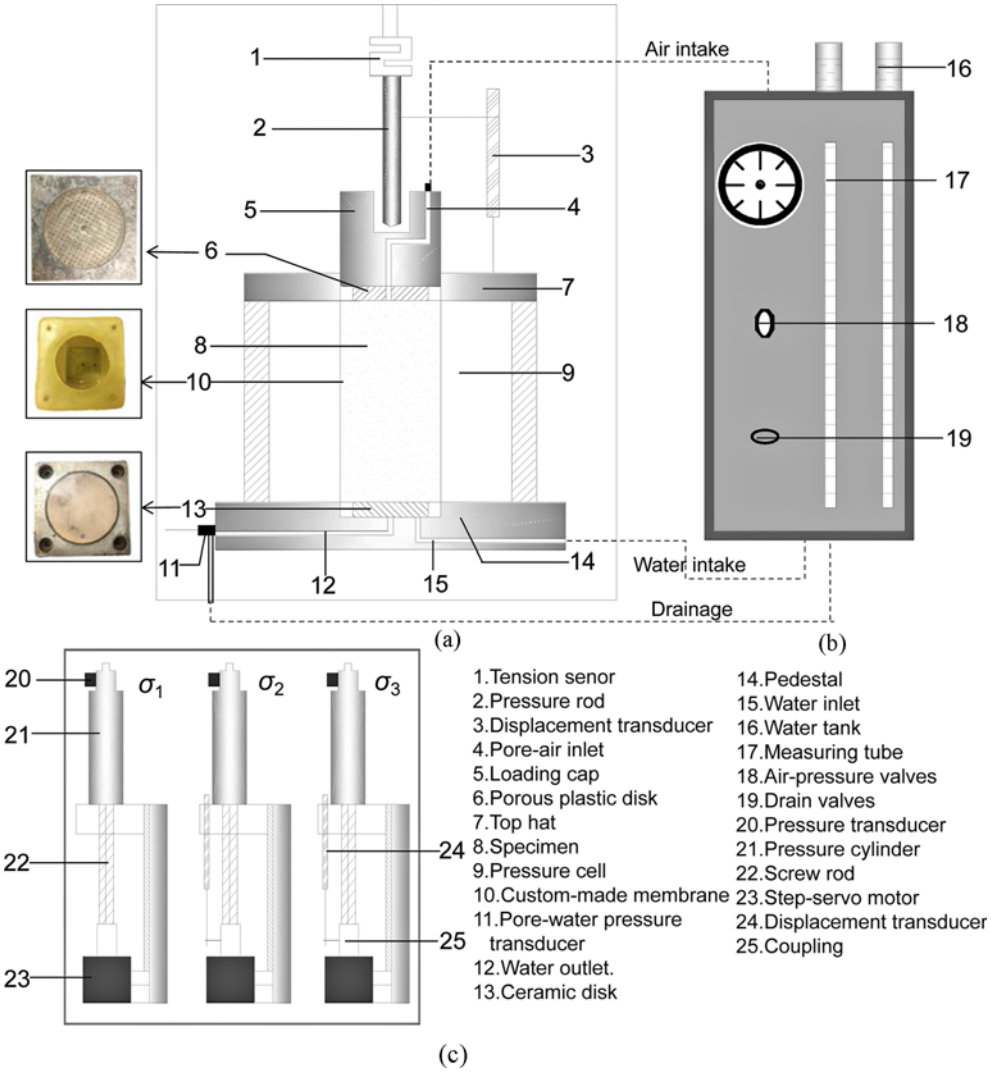

Fig. 5. Schematic of the Suction-Controlled True Triaxial Apparatus: (a) Pressure Chamber, (b) Water/Air Control System, (c) Hydraulic Drive System

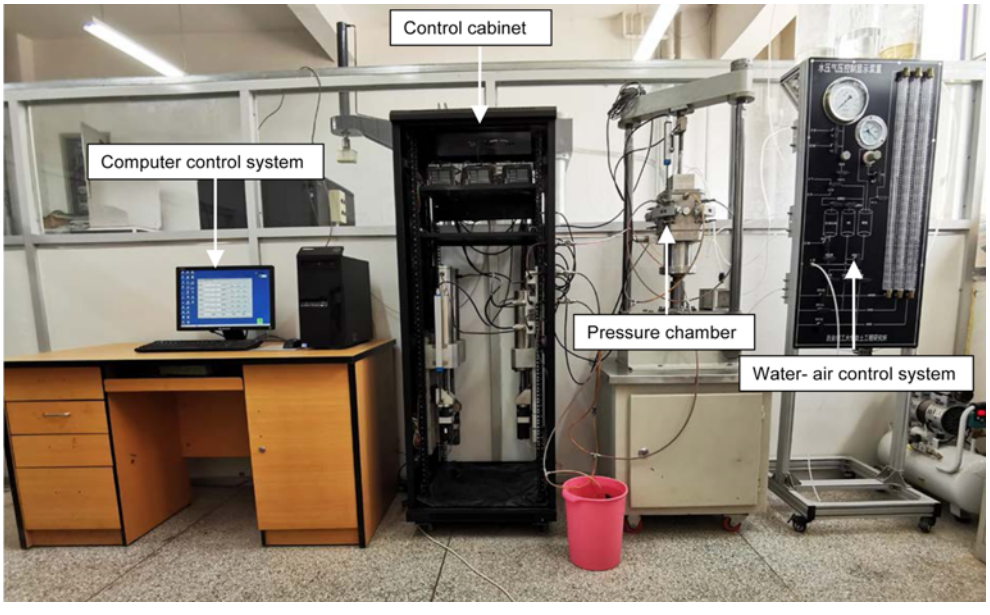

Fig. 6. Panorama of the Suction-Controlled True Triaxial Apparatus

The value of the pore air pressure (u_a) is regulated by the water/gas control system and the value of pore water pressure (u_w) is measured via pressure transducer. In this paper, drainage valves are open (i.e., $u_w = 0$); thus, matric suction is equal to pore-air pressure (i.e., $s = u_a$). Fig. 6 shows a panorama of the fully suction-controlled true triaxial apparatus.

4. Test Programme

Table 2 gives the test programme of consolidation. In this paper, four groups of isotropic consolidation tests were carried out via true triaxial testing under different suction conditions. The loading increments applied to the specimens are detailed in Table 2. An initial suction equilibrium is created in each loess sample before loading. To ensure that the custom-made membrane is close to the specimen, the net mean pressure (p) is maintained at 5 kPa; p is defined in Eq. (1). The equilibrium is achieved when no further change in the water volume of drainage is observed. Then, the equal consolidation stage of the suction-controlled conditions is entered, that is, the net confining pressure is applied incrementally. The standard for the completion of the consolidation stage is that no further volume deformation of the specimen and no further change in the expelled water volume is observed.

Table 3 shows the test programme of the true triaxial test under suction-controlled conditions with different b-values, in which b is defined in Eq. (2). The specimen under a suction of zero ($s = 0$) is fully saturated. A specimen should be saturated before conducting experiments under a suction of zero ($s = 0$). Then, the experiment under a suction of zero is performed in two stages: the consolidation stage and true triaxial shear stage. The process of testing under suction-controlled conditions (s = 100 kPa, 200 kPa, or 300 kPa) is divided into three stages: water-gas equilibrium stage, consolidation stage and shear stage. The first two stages are similar to the abovementioned consolidation tests. True triaxial shear tests of the natural loess are conducted under full drainage conditions. During the shearing process, the matric suction (s) and the net mean stress (p) are kept at a constant value at the same time. The shear tests are carried out at a constant strain rate of 0.0107%/min along the vertical direction.

$$p = \frac{(\sigma_1 + \sigma_2 + \sigma_3)}{3} - u_a \tag{1}$$

$$b = (\sigma_2 - \sigma_3) / (\sigma_1 - \sigma_3) \tag{2}$$

Table 2. Consolidation Test Programme

Matric suction, s/kPa	Loading procedure, p/kPa
0	25, 50, 100, 200, 300, 400, 500, 600
100	25, 50, 100, 150, 200, 300, 400, 500, 600, 700, 800
200	25, 50, 100, 200, 300, 400, 600, 800
300	25, 50, 100, 200, 300, 400, 500, 600, 700, 800

Table 3. Suction-Controlled True Triaxial Test Programme

Matric suction, s/kPa	Consolidation net confining pressure, p/kPa	Intermediate principal stress parameter, b				
0	100, 200, & 300	0	0.25	0.5	0.75	1
100	100, 200, & 300	0	0.25	0.5	0.75	1
200	100, 200, & 300	0	0.25	0.5	0.75	1
300	100, 200, & 300	0	—	—	—	—

5. Experimental Results and Discussion

5.1 Consolidation Yield Characteristics

The isotropic compression tests of unsaturated loess are carried out via a true triaxial apparatus under suction-controlled conditions. The corresponding pore ratio (e) is calculated from the compression of the specimen under each net mean press (p). Thus, the compression curve of unsaturated loess is obtained at different matric suctions under isotropic consolidated conditions. Fig. 7 shows the consolidation curves of the unsaturated natural loess in true triaxial tests under suction-controlled conditions. The net confining stress (p) applied on the soil increases, which can gradually make the soil compacted, as a result of the decrease in the void ratio (e). Under the same net compression stress condition, the rate of change in the void ratio decreases as the matric suction increases. This decrease is due to the existence of matric suction, which strengthens the soil skeleton along the contraction membrane on interfacial surface between pore gas and water. Moreover, the bound water between the soil particles connects the particles of the soil skeleton, and the water/gas is resistant to the additional stress. However, when the matric suction is small, the curvature of the contraction membrane decreases, and the

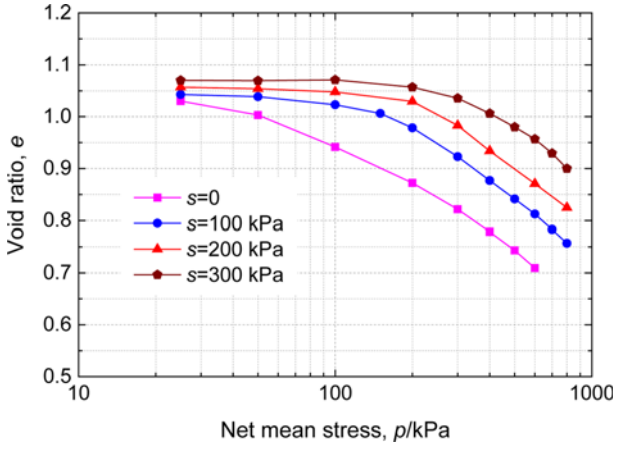

Fig. 7. Consolidation Curves from the True Triaxial Tests under Suction-Controlled Conditions

bound water film between soil particles thickens, reducing the coupling effect between the soil particles.

Comparing the e-log p curves for different matric suctions, they are all composed of gentle and steep declining sections because the natural soil maintains a certain structural strength. When the matric suction is higher, the initial structural strength of the soil is stronger, and thus, the gentle section is longer. With the decrease in suction, the initial structural behaviour becomes weak; consequently, the gentle section shortens and is even eliminated, while the steep section increases. When the net mean pressure is lower than the structural strength of soil, the soil structure has not been destroyed; thus the change in the void ratio is small and the curves present gentle sections. Meanwhile, the pressure is greater than the structural strength, and the soil skeleton and the connections between particles are damaged. With increasing pressure, the net yield stress is reached. Then, sliding between particles occurs, and the structure of the soil skeleton collapses, resulting in a large deformation.

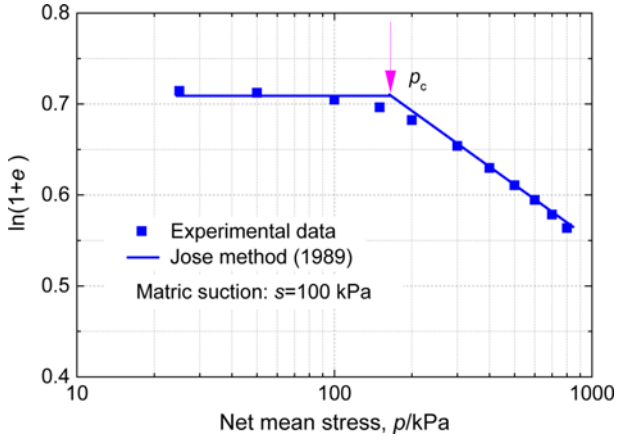

Fig. 8. Jose Method (Jose et al., 1989)

Table 4. Consolidation Net Yield Stress of Unsaturated Loess

Matric suction, s/kPa	Net yield stress, p_c/kPa
0	52
100	170
200	254
300	313

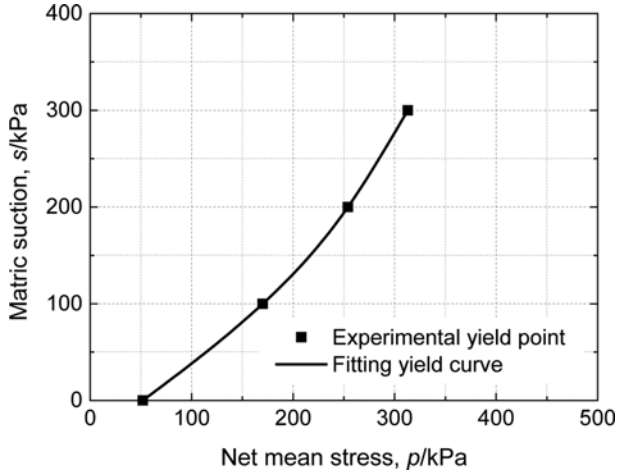

Fig. 9. Loading-Collapse (LC) Yield Curve of Natural Loess

The consolidation net yield stress can be determined by the Jose method (Jose et al., 1989; Junior and Pierce, 1995). The Jose method is illustrated in Fig. 8, taking the test result under a suction of 100 kPa as an example. Then, the other results of the consolidation experiments are processed in the same way. Thus, the consolidation net yield stress under different suctions is obtained and given in Table 4. The data in Table 4 are drawn in the p-s plane; thus, a loading-collapse (LC) yield curve of natural loess can be obtained, as shown in Fig. 9.

5.2 Stress-Strain Behaviour of Natural Loess

5.2.1 Stress-Strain Response of Shearing

True triaxial shear tests are performed under suction-controlled conditions. During the shearing process, both the matric suction (s) and the net mean stress (p) are controlled to be constant. The two important parameters in the test process are the matric suction (s), which can reflect the unsaturated characteristics of the soil, and the intermediate principal stress parameter (b), which can reflect the contribution of the principal stress in the true triaxial shear process. A series of forty-eight consolidated drained tests under suction-controlled conditions were conducted on specimens of natural loess in a true triaxial apparatus. After completion of the water-gas equilibrium stage, specimens were subjected to a consolidation stage under a constant suction condition (s = 100 kPa, 200 kPa or 300 kPa). Then, specimens were subjected to a shearing stage under different b-values, keeping the matric suction (s) and net mean stress (p) at a constant value.

When the b-value is equal to 0, the intermediate principal stress (σ_2) is equal to the minor principal stress (σ_3), and they decrease synchronously. This stress path is the same as that used in conventional compression triaxial testing. When b is 1, the major principal stress (σ_1) is the same as the intermediate principal stress (σ_2). In this case, the intermediate and minor principal stresses increase synchronously. When b is 0.5, the intermediate principal stress (σ_2) remains unchanged. The major principal stress (σ_1) increases while the minor principal stress (σ_3) decreases, but they change at the same increment (i.e., $\Delta\sigma_1 = -\Delta\sigma_3$). During the entire loading process for different b-values, the minor principal stress (σ_3) always decreases, while the intermediate principal stress (σ_2) first decreases (when $b <$ 0.5) and then increases (when $b > 0.5$).

Figures 10 to 12 show the measured curves from experimental results, indicating the deviatoric stress (q) versus deviatoric strain (ε_d); q is defined in Eq. (3), and ε_d is defined in Eq. (4):

$$q = \frac{1}{\sqrt{2}}\sqrt{(\sigma_1-\sigma_2)^2+(\sigma_2-\sigma_3)^2+(\sigma_3-\sigma_1)^2} \tag{3}$$

$$\varepsilon_d = \frac{\sqrt{2}}{3}\sqrt{(\varepsilon_1-\varepsilon_2)^2+(\varepsilon_2-\varepsilon_3)^2+(\varepsilon_3-\varepsilon_1)^2} \tag{4}$$

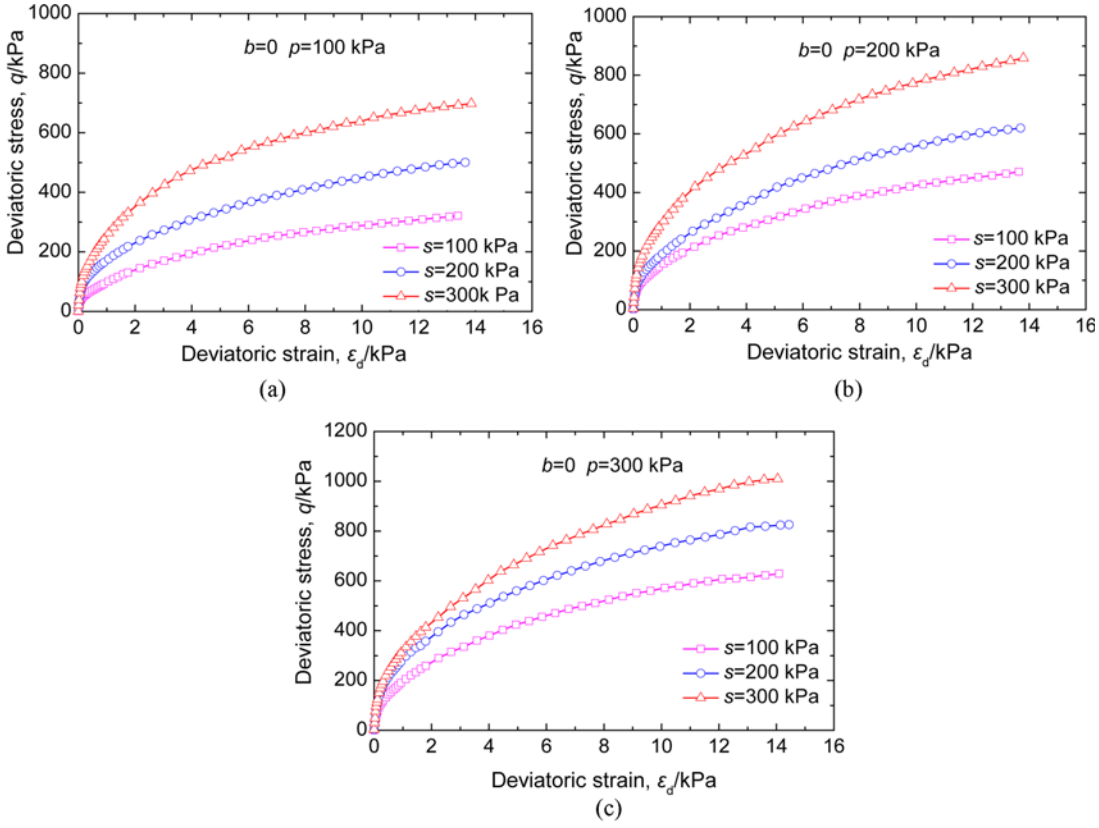

Fig. 10. Stress-Strain Responses for Different Suctions with the Same b-Value: (a) $p = 100$ kPa, (b) $p = 200$ kPa, (c) $p = 300$ kPa

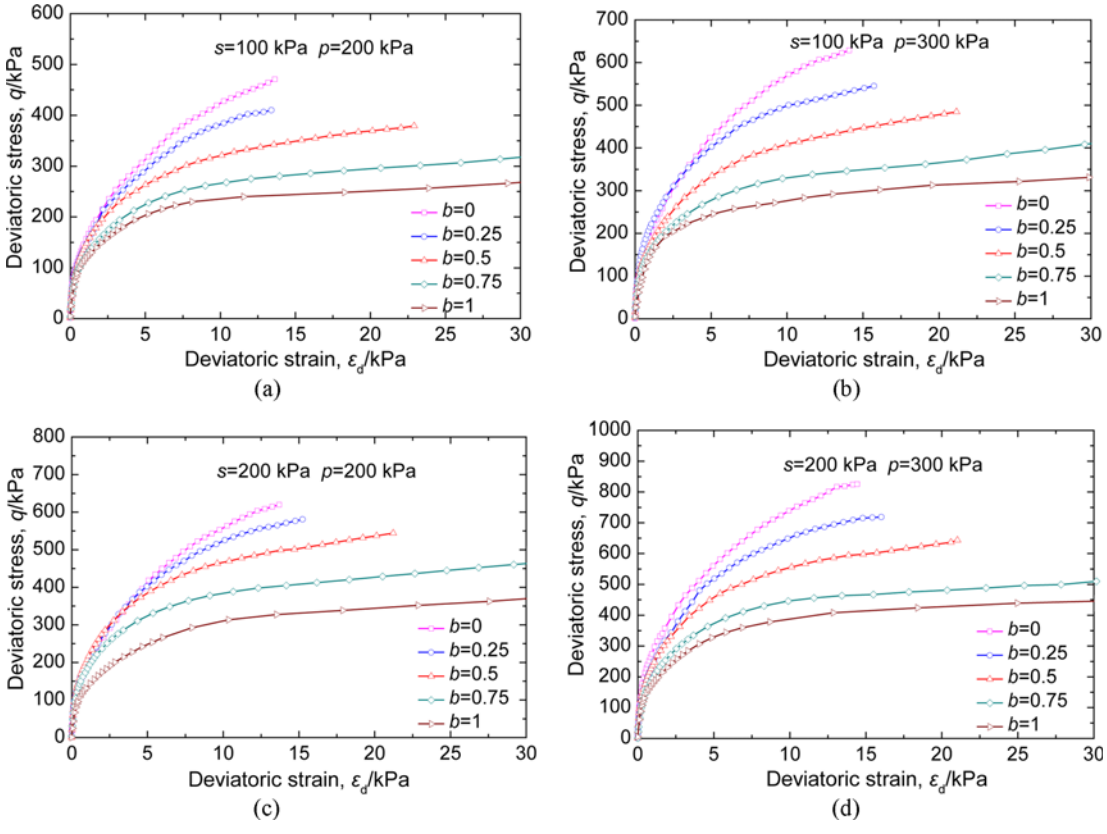

Fig. 11. Stress-Strain Response for Different Values of b: (a) $s = 100$ kPa, $p = 200$ kPa, (b) $s = 100$ kPa, $p = 300$ kPa, (c) $s = 200$ kPa, $p = 200$ kPa, (d) $s = 200$ kPa, $p = 300$ kPa

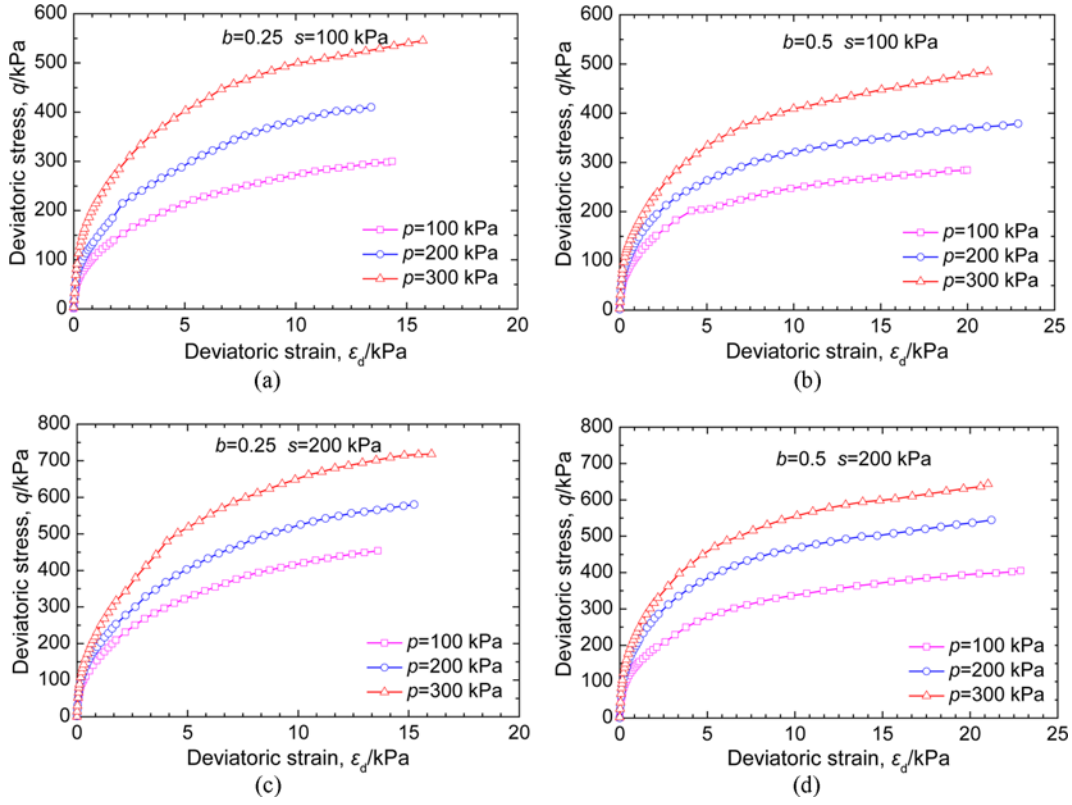

Fig. 12. Stress-Strain Response for Different Net Mean Stresses: (a) b = 0.25, s = 100 kPa, (b) b = 0.5, s = 100 kPa, (c) b = 0.25, s = 200 kPa, (d) b = 0.5, s = 200 kPa

where ε_1 is the major principal strain; ε_2 is the intermediate principal strain; and ε_3 is the minor principal strain.

In all cases, the stress-strain curves of natural loess show strain-hardening characteristics. As can be seen, the deviatoric stress (q) increases with the increase of the deviatoric strain (ε_d). Fig. 10 presents the stress-strain responses of the tested soil for different matric suctions under the same value of b. As Figs. 10(a) – 10(c) show, under different net mean stresses (p = 100 kPa, 200 kPa and 300 kPa), the matric suction exhibits a significant influence on the stress-strain-strength response of the natural loess. Fig. 10 shows that the deviatoric stress (q) increases considerably with matric suction (s); thus, matric suction (s) makes a great effect on the shear strength for unsaturated natural loess.

Figure 11 presents the stress-strain responses for different b-values. Figs. 11(a) – 11(b) give the measured curves of the deviatoric stress (q) versus deviatoric strain (ε_d) for a suction of 100 kPa under different net mean stresses (p = 200 kPa and p = 300 kPa), respectively; Figs. 11(c) – 11(d) give the results of a suction of 200 kPa under different net mean stresses (p = 200 kPa and p = 300 kPa), respectively. Fig. 11 indicates that the deviatoric stress (q) decreases with the b-value. The stress-strain curve is transformed from the strain-hardening type to the ideal type as b increases from small to large. The measured curves in Fig. 11 indicate that the stress-strain-strength response is dependent on the b-value.

Figure 12 shows the stress-strain responses for different net mean stresses (p). Figs. 12(a) – 12(b) give the measured curves for b-values of 0.25 and 0.5 under a matric suction of 100 kPa, respectively. Figs. 12(c) – 12(d) also show the results under a suction of 200 kPa.With the increase in the net mean pressure, the curve shifts up, which indicates that an increase in the consolidation net confining pressure can improve the soil strength because the soil compacts under the consolidation net confining pressure.

5.2.2 Normalization of the Stress-Strain Curves

The test results with a matric suction of 200 kPa are analysed as an example. The curves of the stress ratio ($\eta = q/p$) versus deviatoric strain (ε_d) are presented in Fig. 13. The curve with a lower net mean pressure always plots above the curve with a higher net mean pressure. The lower the consolidated net confining pressure is, the higher the stress ratio is, according to the definition of the stress ratio. The difference between the curves at net confining pressures of 100 kPa and 200 kPa is greater than that between the curves at 200 kPa and 300 kPa. The curves for the consolidated net mean pressure of 100 kPa are significantly higher than those of the other two groups.

The stress ratio (η) is divided by the stress ratio at the point of failure (η_f); in this way, the experimental data under different net mean pressures (p) are normalized and are given in Fig. 14. As shown in Fig. 14, for the same intermediate principal stress parameter (b), the experimental data under different net mean

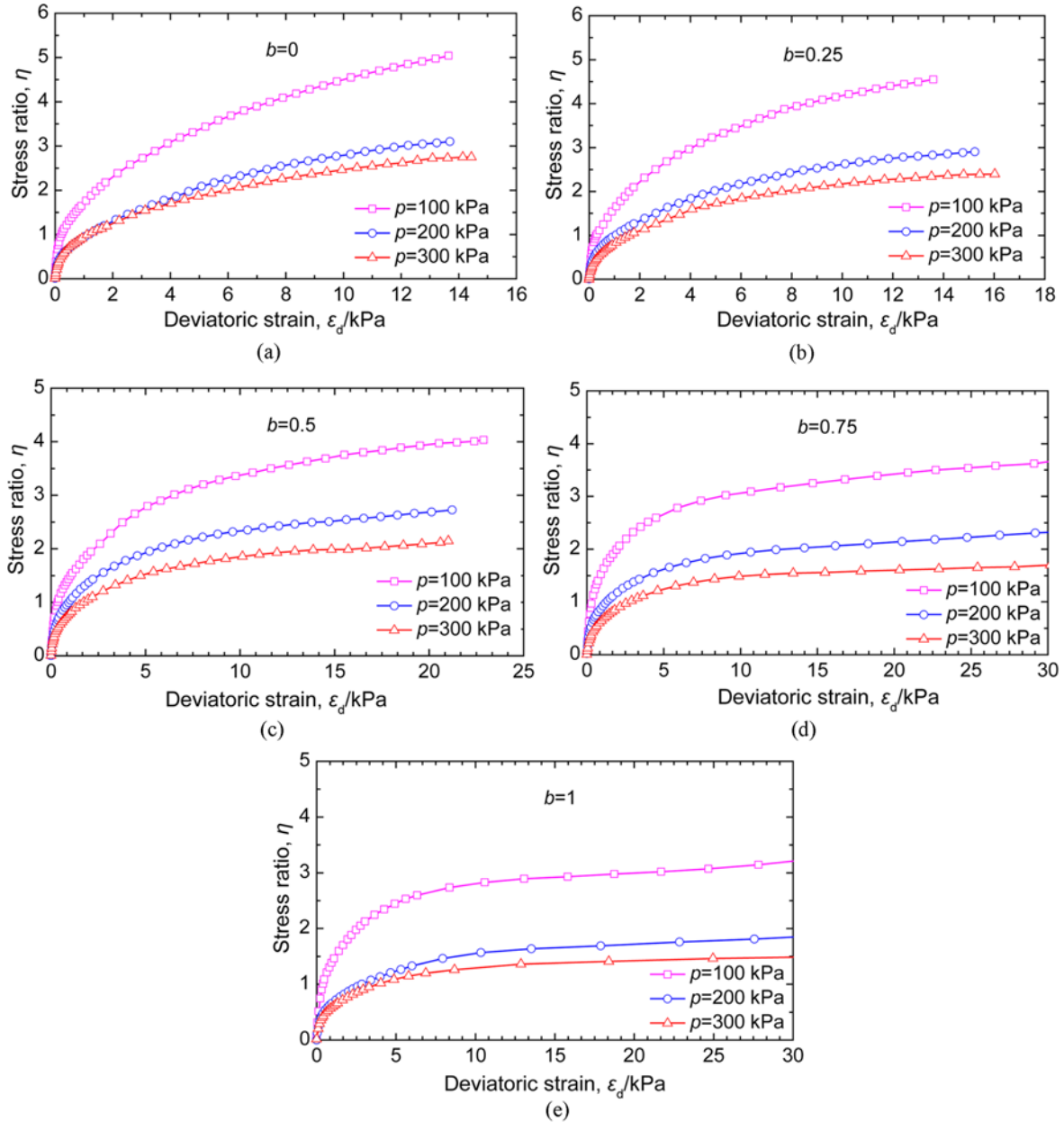

Fig. 13. Stress Ratio versus Deviatoric Strain under a Suction of 200 kPa for Different *b*-Values: (a) $b = 0$, (b) $b = 0.25$, (c) $b = 0.5$, (d) $b = 0.75$, (e) $b = 1$

pressures (p) are centralized after normalization, which indicates that the results of the normalization are good. The data points after normalization can be fitted by the same curve. Therefore, for the same intermediate principal stress parameter (b), there is a corresponding relationship between the normalized stress ratio (η/η_f) and the deviatoric strain (ε_d). This relationship can be expressed by Eq. (5).

$$\eta / \eta_f = \frac{\varepsilon_d}{a + k\varepsilon_d} \tag{5}$$

where η is the stress ratio ($\eta = q/p$); η_f is the stress ratio at the point of failure; ε_d is the deviatoric strain; and a and k are the fitting parameters. Eq. (5) can be written as Eq. (6).

$$\frac{\varepsilon_d}{\eta / \eta_f} = a + k\varepsilon_d \tag{6}$$

Equation (6) shows that the relationship between $\frac{\varepsilon_d}{\eta / \eta_f}$ and ε_d is linear. For this relationship, a is the intercept, and k is the slope of the line. Therefore, the parameters in Eq. (5) can be obtained for different intermediate principal stress parameter values. The normalized curves are independent of the net confining pressure and depend on only the intermediate principal stress parameter (b). With the increase in the b-value, the curves

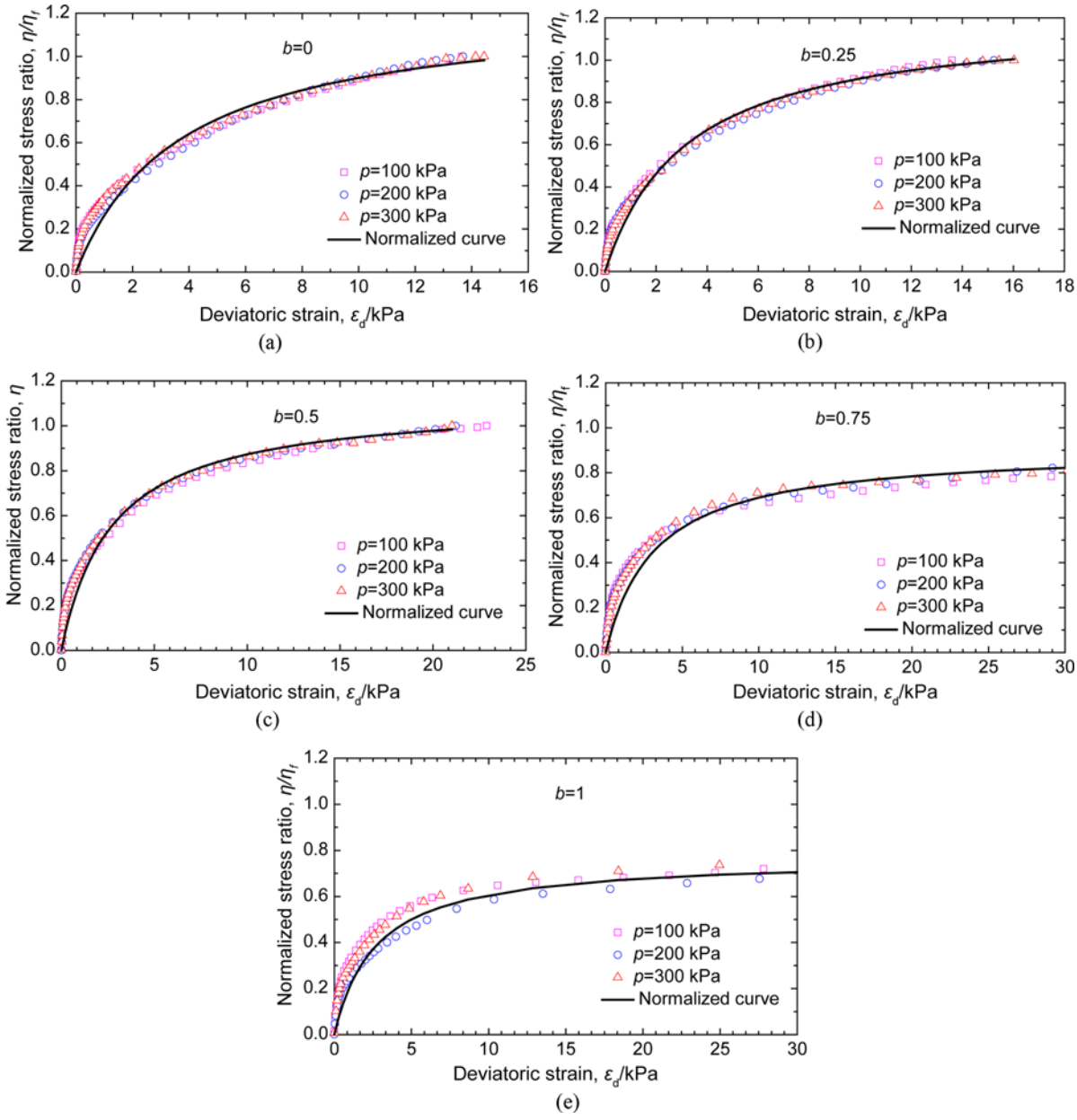

Fig. 14. Normalized Stress Ratio versus Deviatoric Strain under a Suction of 200 kPa for Different *b*-Values: (a) $b = 0$, (b) $b = 0.25$, (c) $b = 0.5$, (d) $b = 0.75$, (e) $b = 1$

change from a hardening type to a more ideal elastic-plastic type.

5.3 Failure Envelopes of Unsaturated Natural Loess

The stress-strain curves of the test loess in this experiment present strain-hardening, and thus, the failure stress is defined as the stress when the axial strain is 15%. According to the failure stress under different mean stresses, the failure strength line for the same intermediate principal stress parameter (b) can be obtained, which is a critical state line (CSL) of failure. Fig. 15 shows the failure line of the unsaturated natural loess in the p-q plane with the same b-value under different matric suctions. Figs. 15(a) – 15(e) present the results with b values of 0, 0.25, 0.5, 0.75 and 1.

Figure 15 shows that the failure strength of unsaturated intact loess increases with increasing net mean stress (p) at the same b and s values. Failure points of different net mean stresses (p) at the same b and s values can be well fitted by a straight line, which is a failure line or CSL. In summary, the CSL undergoes an upward shift with the increase in matric suction at the same b value. However, the slope of the failure line remains constant at the same value of b.

Additionally, the failure line of all of the saturated loess specimens passes through the origin of the coordinate system. Therefore, matric suction (s) makes a considerable effect on the CSL of natural loess. The existence of matric suction (s) strengthens the soil to some extent.

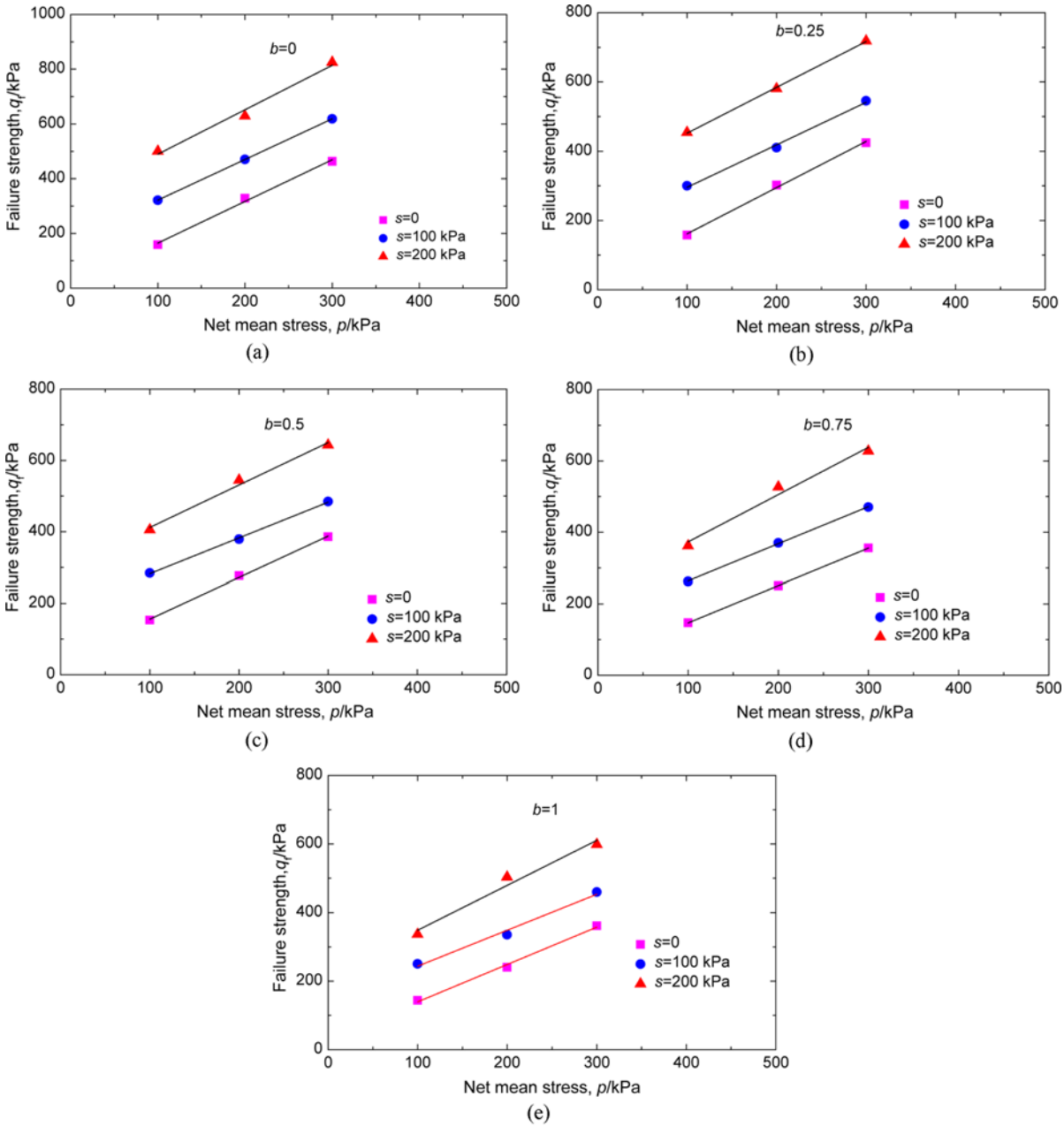

Fig. 15. Failure Lines of the Unsaturated Natural Loess in the p-q Plane for Different b-Values: (a) $b = 0$, (b) $b = 0.25$, (c) $b = 0.5$, (d) $b = 0.75$, (e) $b = 1$

Figure 16 shows the failure surfaces of unsaturated undisturbed loess on the π-plane $((\sigma_1 - u_a):(\sigma_2 - u_a):(\sigma_3 - u_a))$ under different net mean pressures of 100 kPa, 200 kPa and 300 kPa. As Figs. 16(a) – 16(c) show, under different net mean pressures, the failure envelopes are irregular and cone-shaped. With the increase in matric suction, the failure surface gradually expands. The matric suction has a considerable influence on the position, size and shape of the failure surface of natural loess. A comparison of several different failure criteria (Mohr-Coulomb failure criterion, extended von Mises failure criterion and Lade-Duncan failure criterion) based on the experimental data are presented in Fig. 17, taking the experimental data of $s = 100$ kPa and $p = 300$ kPa as an example. As can be observed, the experimental result of natural loess via suction-controlled true triaxial testing exhibits more agreement with the failure criterion of Lade-Duncan. In the Mohr-Coulomb criterion, only σ_1 and σ_3 acting on the element are considered, but σ_2 is not taken into consideration, thus the predicted results are more conservative. While in the Extended von Mises criterion, the effect of σ_2 is considered. But it is supposed that the effect of σ_2 on material strength is the same as that of σ_3, which exaggerates the effect of σ_2, leading to the predicated result to be more dangerous.

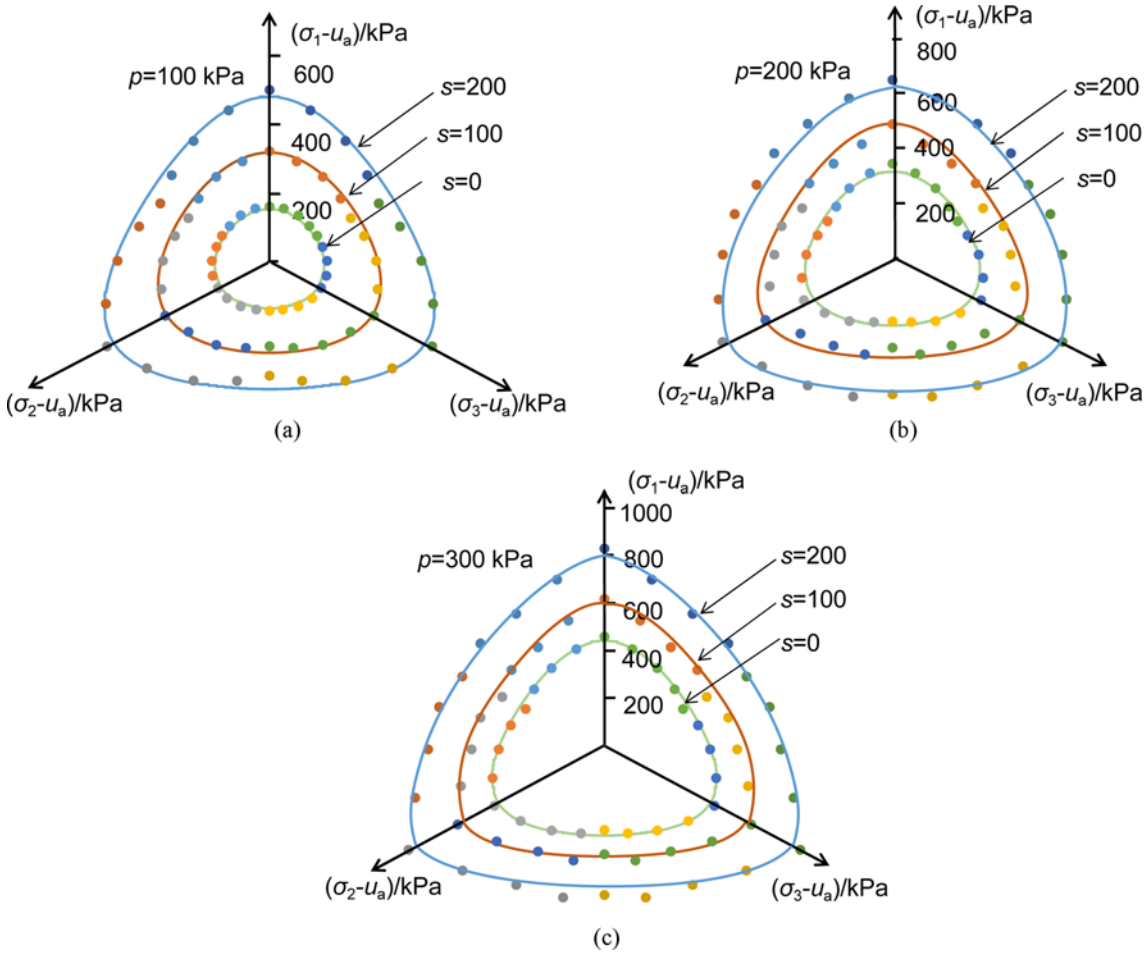

Fig. 16. Failure Surfaces in the π-Plane under Different Net Mean Pressures: (a) 100 kPa, (b) 200 kPa, (c) 300 kPa

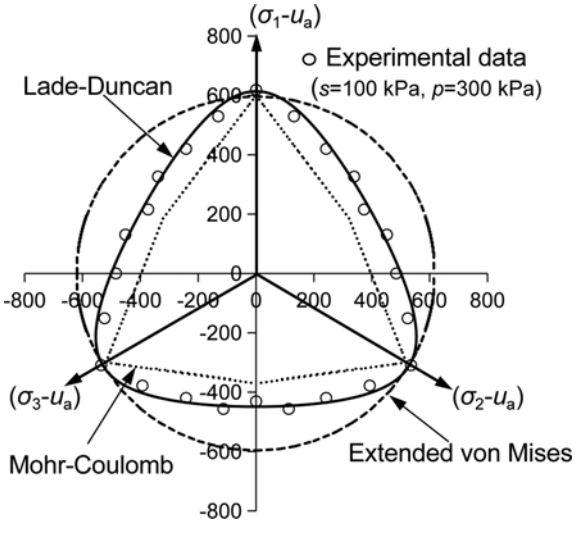

Fig. 17. Comparison of Several Different Failure Criteria

5.4 Effect of Matric Suction on Shear Strength Parameters

It is more adopted double independent stress state variables to investigate the strength characteristics in unsaturated soil. It has been suggested the net normal stress $(\sigma - u_a)$ as one stress state variable and matric suction $(u_a - u_w)$ as the other to used to define the stress state in unsaturated soil by Fredlund and Morgenstern (1977). Then, a shear strength equation has been established on the basis of these two stress state variables (Fredlund et al., 1978). The shear strength equation is defined in Eq. (7):

$$\tau_f = c' + (\sigma - u_a)_f \tan\phi' + (u_a - u_w)_f \tan\phi^b \tag{7}$$

where τ_f is shear strength at failure; c' is effective cohesion; $(\sigma - u_a)_f$ is net normal stress at failure; ϕ' is the internal friction angle with regard to net normal stress variable; $(u_a - u_w)_f$ is the matric suction at failure; and ϕ^b is the friction angle with regard to suction. Eq. (7) can be further written as Eq. (8):

$$\tau_f = c + (\sigma - u_a)_f \tan\phi' \tag{8}$$

where c is called the total cohesion intercept and defined in Eq. (9) (Fredlund and Rahardjo, 1993).

$$c = c' + (u_a - u_w)_f \tan\phi^b \tag{9}$$

Figure 18 gives the Mohr circles obtained at the failure state under suction-controlled conditions at different net confining pressures when $b = 0$. In the $b = 0$ test, the intermediate principal stress (σ_2) and the minor principal stress (σ_3) are equal, which is

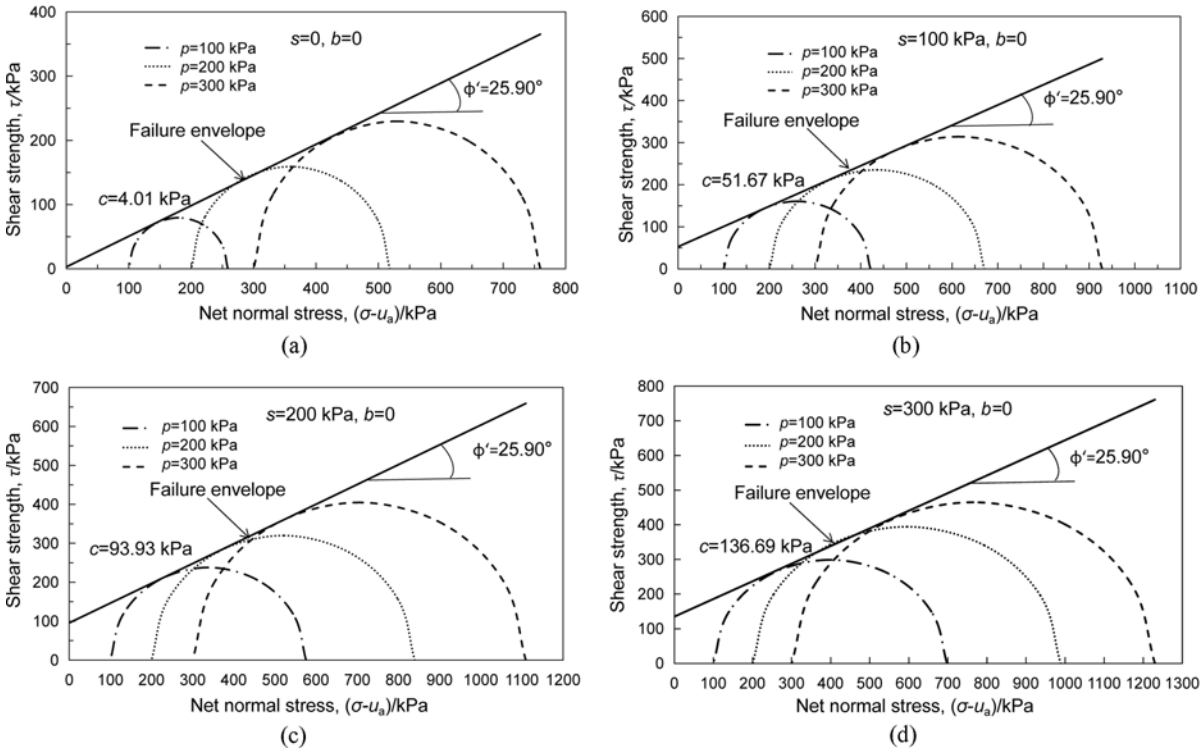

Fig. 18. Mohr Circles under Different Suctions of: (a) 0, (b) 100 kPa, (c) 200 kPa, (d) 300 kPa

Table 5. Parameters of Shear Strength

Matric suction, s/kPa	Net confining pressure, p/kPa	Intermediate principal stress parameter, b	Total cohesion intercept, c/kPa	Internal friction angle, ϕ'/°		Friction angle with respect to suction, ϕ^b/°
0	100, 200, & 300	0	4.01(c')	25.54	Average 25.90	—
100	100, 200, & 300	0	51.67	25.70		25.50
200	100, 200, & 300	0	93.93	26.31		24.22
300	100, 200, & 300	0	136.69	26.03		23.87

consistent with a conventional triaxial compression test. As shown in Fig. 19, the internal friction angle (ϕ') indicates the slope of the failure envelope, which has a negligible change under different matric suctions (s). This result indicates that the strength parameter of the internal friction angle is independent of the matric suction and net confining pressure, and thus, the averaged value under different suctions is taken as the internal friction angle. With increasing matric suction, the failure envelope shifts upward. The vertical intercept of this line is the total cohesion intercept (c), which shows a marked increase with matric suction. The internal friction angle (ϕ'), the total cohesion intercept (c) and the friction angle with regard to suction (ϕ^b) are listed in Table 5. The friction angle with regard to suction (ϕ^b) is derived from Eq. (9) and reflects the rate at which the unsaturated shear strength increases with the matric suction. As shown in Table 5, ϕ^b of the unsaturated loess decreases with s. The test results of the unsaturated loess show that the value of ϕ^b is less than the value ϕ'. The results are consistent with those of previous studies on suction-controlled triaxial tests (e.g., Fredlund and Rahardjo, 1993; Patil, 2017).

The shear strength parameters under different intermediate principal stress parameter values are obtained by a method similar to that described above. The values of the strength parameters are summarized in Table 6, and the relationship curves of the strength parameters with the intermediate principal stress parameter under different matric suctions are shown in Fig. 19. As summarized in Table 6 and Fig. 19, the total cohesion (c) and friction angle with regard to suction (ϕ^b) are related to not only matric suction (s) but also the intermediate principal stress parameter (b). The total cohesion increases with increasing matric suction but increases and then decreases with an increasing b-value, peaking between 0.25 and 0.5. The friction angle with regard to suction presents a similar changing trend with matric suction and the intermediate principal stress parameter. While the internal friction angle (ϕ') is independent of suction, it varies with the principal stress parameter (b). The peak of the internal friction angle (ϕ') is between 0.5 and 0.75.

Table 6. The Strength Parameter Results for Different Values of b

Matric suction, s/kPa	Intermediate principal stress parameter, b	Total cohesion intercept, c/kPa	Internal friction angle, ϕ'/°	Friction angle with respect to suction, ϕ^b/°
0	0	4.01(c')	25.90	—
	0.25	6.23(c')	25.58	—
	0.5	6.62(c')	26.63	—
	0.75	4.66(c')	25.80	—
	1	3.11(c')	25.47	—
100	0	51.67	25.90	25.50
	0.25	54.19	25.58	25.62
	0.5	53.04	26.63	24.90
	0.75	46.39	25.80	22.65
	1	39.37	25.47	19.93
200	0	93.93	25.90	24.22
	0.25	95.92	25.58	24.15
	0.5	96.70	26.63	24.24
	0.75	84.62	25.80	21.79
	1	73.7	25.47	19.44
300	0	136.68	25.90	23.87

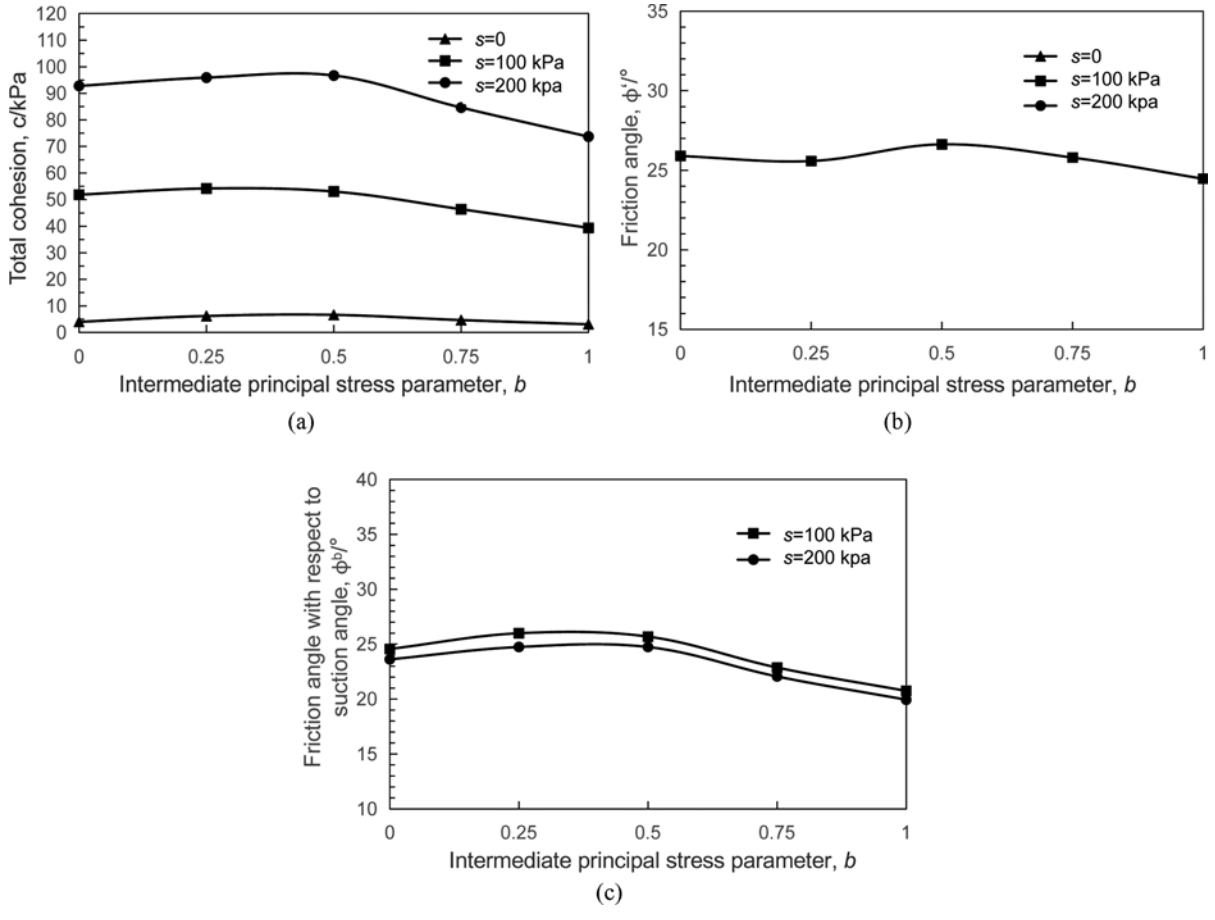

Fig. 19. Curves of the Shear Strength Parameters versus b-Value: (a) c versus b, (b) ϕ' versus b, (c) ϕ^b versus b

5.5 Comparison and Discussion

As for the research on the true triaxial test of controlled suction, some scholars have also performed some research on other soil types. For example, Matsuoka et al. (2002) discussed the stress-strain responses of unsaturated silt via a fully rigid-boundary true triaxial device. However, due to the limitation of the rigid

boundary, the true triaxial tests were only carried out where the Lode angle was not greater than 30º (i.e., $b \leq 0.5$); moreover, since the method of $s = -u_w$ was adopted in the test, the controlled matric suction was also less than 100 kPa. Macari and Hoyos (2001) and Macari et al. (2003) investigated the mechanical behaviour of unsaturated low-plasticity silty sand via a five flexible-boundary true triaxial apparatus. The range of suction controlled in this experiment was wider, and tests with Lode angles of 0, 30º and 60º (i.e., $b = 0$, 0.5 and 1) were conducted in this experiment. Meanwhile, in this paper, five different b-value (i.e., $b = 0$, 0.25, 0.5, 0.75 and 1) tests under the suction-controlled condition were conducted on natural loess. More stress paths were adopted in this experiment, which can simulate a more complex stress loading mode. The natural loess specimens were taken for testing, which is closer to the characteristics of soil exhibited in engineering practice. The shear strength of unsaturated silt measured from the fully rigid-boundary true triaxial device nearly agreed with the extended SMP criterion (Matsuoka et al., 2002) under the suction-controlled condition. Meanwhile, the shear strength of unsaturated low-plasticity silty sand obtained by a five flexible-boundary true triaxial device (Macari and Hoyos, 2001; Hoyos et al., 2012) and the shear strength of unsaturated loess obtained by the rigid-boundary true triaxial device show more agreement with Lade-Duncan failure criterion.

6. Conclusions

Several groups of suction-controlled drained true triaxial trials were conducted on unsaturated natural loess with five different b-values. The soil response was investigated by testing specimens of natural loess at different four matric suctions (s) and different three net mean stresses (p). The main conclusions of this study from the results of 52 trials on intact loess under suction-controlled conditions are as follows:

1. Four groups of isotropic consolidation trails were performed on natural loess under different matric suctions via a true triaxial apparatus. The rate of change in void ratio of the tested loess decreases with the increase of matric suction. The consolidation net yield stresses of the tested loess corresponding to 0, 100, 200 and 300 kPa are 52, 170, 270, and 313 kPa, respectively, increasing nonlinearly in the p-s plane.
2. The measured stress-strain curves from the true triaxial shear tests of natural loess under suction-controlled conditions all show strain-hardening characteristics. The deviatoric stress (q) clearly decreases as the b-value increases. The stress-strain curve is transformed from the strain-hardening type to the ideal type as b increases from a small value to a large value.
3. The measured stress-strain curves for the same matric suction and the intermediate principal stress parameter but under different net mean stresses can be normalized through the normalized stress ratio (η/η_f), which can then be normalized to a hyperbolic curve with an expression of $\eta/\eta_f = \varepsilon_d/(a+k\varepsilon_d)$.
4. Matric suction (s) makes a considerable effect on the stress-strain responses of unsaturated natural loess. The deviatoric stress (q) increases considerably with matric suction (s). Failure envelopes on the p-q plane of unsaturated natural loess appear as straight lines under the same suction. The failure lines for different matric suctions with the same b-value are parallel. The failure envelopes in the p-q plane for different intermediate principal stress parameter values intersect at one point along the p axis under the same matric suction.
5. The failure envelopes of the unsaturated natural loess on the π-plane present irregular cone shapes under a suction-controlled stress path. The matric suction takes a significant influence on the position, size and shape of the failure surface of natural loess.
6. The total cohesion (c) and friction angle with regard to suction (ϕ^b) are related not only to the matric suction (s) but also to the b-value. The total cohesion increases with matric suction, while it increases and then decreases with the b-values. Although the internal friction angle (ϕ') is independent of matric suction (s), it varies with the principal stress parameter (b).

Acknowledgements

This research was accomplished under the financial support from the National Natural Science Foundation of China (Grant Nos. 11572245 and 41272320). This support is gratefully acknowledged.

ORCID

Fang Zheng https://orcid.org/0000-0003-1503-3174
Shengjun Shao https://orcid.org/0000-0001-6861-5149

References

Chen CL, Zhang DF, Dong YZ, Chen H, Yu DB, Xue JX (2014) Suction and mechanical behaviours of unsaturated intact loess from constant water content triaxial tests. *Chinese Journal of Geotechnical Engineering* 36(7):1195-1202, DOI: 10.11779/CJGE201407002 (in Chinese)

Choi C, Arduino P, Harney MD (2008) Development of a true triaxial apparatus for sands and gravels. *Geotechnical Testing Journal* 31(1):32-44, DOI: 10.1520/GTJ100217

Derbyshire E (2001) Geological hazards in loess terrain, with particular reference to the loess areas of China. *Earth-Science Reviews* 54(1-3):231-260, DOI: 10.1016/S0012-8252(01)00050-2

Fan XM, Xu Q, Scaringi G, Li S, Peng DL (2017) A chemo-mechanical insight into the failure mechanism of frequently occurred landslides in the Loess Plateau, Gansu Province, China. *Engineering Geology* 228(13):337-345, DOI: 10.1016/j.enggeo.2017.09.003

Fredlund DG, Morgenstern NR (1977) Stress state variables for unsaturated soils. *Journal of the Geotechnical Engineering Division* 103(5):447-466

Fredlund DG, Morgenstern NR, Widger RA (1978) The shear strength of unsaturated soils. *Canadian Geotechnical Journal* 15(3):313-321, DOI: 10.1139/t78-029

Fredlund DG, Rahardjo H (1993) Soil mechanics for unsaturated soils. Wiley & Sons, Inc., Hoboken, NJ, USA

Gao DH, Chen ZH, Guo N, Zhu YP, Hu SX, Yao ZH (2017) The influence of dry density and matric suction on the deformation and the strength characteristics of the remolded loess soils. *Chinese Journal of Rock Mechanics and Engineering* 36(3):736-744, DOI: 10.13722/j.cnki.jrme.2015.1761 (in Chinese)

Gibbs HJ, Holland WY (1960) Petrographic and engineering properties of loess. Technical Information Branch, Denver, CO, USA, 1-37

Hambly EC (1969) A new true triaxial apparatus. *Geotechnique* 19(2):307-309, DOI: 10.1680/geot.1969.19.2.307

Hoyos LR, Macari EJ (2001) Development of a stress/suction-controlled true triaxial testing device for unsaturated soils. *Geotechnical Testing Journal* 24(1):5-13, DOI: 10.1520/GTJ11277J

Hoyos LR, Perez-Ruiz DD, Puppala AJ (2012) Refined true triaxial apparatus for testing unsaturated soils under suction-controlled stress paths. *International Journal of Geomechanics* 12(3):281-291, DOI: 10.1061/(ASCE)GM.1943-5622.0000138

Ibsen LB, Praastrup U (2002) The danish rigid boundary true triaxial apparatus for soil testing. *Geotechnical Testing Journal* 25(3):254-265, DOI: 10.1520/GTJ11096J

Jiang MJ, Shen ZJ (1998) Preparation of artificial structured collapsible loess and its behavior in oedometer test. Proceedings of 2nd international conference on unsaturated soils, August 27-30, Beijing, China

Jiang MJ, Zhang FG, Hu HJ, Cui YJ, Peng JB (2014) Structural characterization of natural loess and remolded loess under triaxial tests. *Engineering Geology* 181(1):249-260, DOI: 10.1016/j.enggeo.2014.07.021

Jose BT, Sridharan A, Abraham BM (1989) Log-log method for determination of preconsolidation pressure. *Geotechnical Testing Journal* 12(3):230-237, DOI: 10.1520/GTJ10974J

Junior MSD, Pierce FJ (1995) A simple procedure for estimating preconsolidation pressure from soil compression curves. *Soil Technology* 8(2):139-151, DOI: 10.1016/0933-3630(95)00015-8

Kim D, Kang SS (2013) Engineering properties of compacted loesses as construction materials. *KSCE Journal of Civil Engineering* 17(2):335-341, DOI: 10.1007/s12205-013-0872-1

Kirkgard MM, Lade PV (1993) Anisotropic three-dimensional behavior of a normally consolidated clay. *Canadian Geotechnical Journal* 30(5):848-858, DOI: 10.1139/t93-075

Ko HY, Scott RF (1967) A new soil testing apparatus. *Geotechnique* 17(1):40-57, DOI: 10.1680/geot.1967.17.1.40

Li P, Vanapalli S, Li TL (2016) Review of collapse triggering mechanism of collapsible soils due to wetting. *Journal of Rock Mechanics and Geotechnical Engineering* 8(2):256-274, DOI: 10.1016/j.jrmge.2015.12.002

Liu Z, Liu FY, Ma FL, Wang M, Bai XH, Zheng YL, Yin H, Zhang GP (2015) Collapsibility, composition, and microstructure of a loess in China. *Canadian Geotechnical Journal* 53(4):673-686, DOI: 10.1139/cgj-2015-0285

Luo H, Wu FQ, Chang JY, Xu JB (2018) Microstructural constraints on geotechnical properties of Malan loess: A case study from Zhaojiaan landslide in Shaanxi province, China. *Engineering Geology* 236(26):60-69, DOI: 10.1016/j.enggeo.2017.11.002

Macari EJ, Hoyos LR (2001) Mechanical behavior of an unsaturated soil under multi-axial stress states. *Geotechnical Testing Journal* 24(1):14-22, DOI: 10.1520/GTJ11278J

Macari EJ, Hoyos LR, Arduino P (2003) Constitutive modeling of unsaturated soil behavior under axisymmetric stress states using a stress/suction-controlled cubical test cell. *International Journal of Plasticity* 19(10):1481-1515, DOI: 10.1016/S0749-6419(02)00018-9

Matalucci RV, Abdel-Hady M, Shelton JW (1970) Influence of grain orientation on direct shear strength of a loessial soil. *Engineering Geology* 4(2):121-132, DOI: 10.1016/0013-7952(70)90008-6

Matsuoka H, Sun D, Kogane A, Fukuzawa N, Ichihara W (2002) Stress–strain behaviour of unsaturated soil in true triaxial tests. *Geotechnical Testing Journal* 39(3):608-619, DOI: 10.1139/T02-031

Ng CWW, Sadeghi H, Jafarzadeh F (2017) Compression and shear strength characteristics of compacted loess at high suctions. *Geotechnical Testing Journal* 54(5):690-699, DOI: 10.1139/cgj-2016-0347

Patil UD, Puppala AJ, Hoyos LR, Perdarla A (2017) Modeling critical-state shear strength behavior of compacted silty sand via suction-controlled triaxial testing. *Engineering Geology* 231(14):21-33, DOI: 10.1016/j.enggeo.2017.10.011

Phien-Wej N, Pientong T, Balasubramaniam AS (1992) Collapse and strength characteristics of loess in Thailand. *Engineering Geology* 32(1-2):59-72, DOI: 10.1016/0013-7952(92)90018-T

Porter SC (2013) Loess records | China. *Encyclopedia of Quaternary Science* 595-605, DOI: 10.1016/B978-0-444-53643-3.00157-6

Reddy KR, Saxena SK, Budiman JS (1992) Development of a triaxial testing apparatus. *Geotechnical Testing Journal* 15(2):89-105, DOI: 10.1520/GTJ10231J

Rogers CDF, Dijkstra TA, Smalley IJ (1994) Hydroconsolidation and subsidence of loess: Studies from China, Russia, North America and Europe. *Engineering Geology* 37(2):83-113, DOI: 10.1016/0013-7952(94)90045-0

Rousseau DD, Derbyshire E, Antoine P, Hatté C (2007) Loess records | Europe. *Encyclopedia of Quaternary Science* 1440-1456, DOI: 10.1016/B0-44-452747-8/00162-9

Ryashchenko TG, Akulova VV, Erbaeva MA (2008) Loessial soils of Priangaria, Transbaikalia, Mongolia, and Northwestern China. *Quaternary International* 179(1):90-95, DOI: 10.1016/j.quaint.2007.06.035

Shao SJ, Wang Q, Luo AZ, Shao S (2017) True triaxial apparatus with rigid-flexible-flexible boundary and remolded loess testing. *Journal of Testing and Evaluation* 45(3):808-817, DOI: 10.1520/JTE20150177

Sheng CN, Fang XW, Chen ZH (2010) The unsaturated direct shear tests of Q2 loess. *Chinese Journal of Underground Space and Engineering* 6(4):724-728, DOI: 10.3969/j.issn.1673-0836.2010.04.012 (in Chinese)

Sun JM (2002) Provenance of loess material and formation of loess deposits on the Chinese Loess Plateau. *Earth and Planetary Science Letters* 203(3-4):845-859, DOI: 10.1016/S0012-821X(02)00921-4

Tan TK (1988) Fundamental properties of loess from northwestern China. *Engineering Geology* 25(2-4):103-122, DOI: 10.1016/0013-7952(88)90022-1

Van Genuchten MT (1980) A closed-form equation for predicting the hydraulic conductivity of unsaturated soils. *Soil Science Society of America Journal* 44(5):892-898, DOI: 10.2136/sssaj1980.03615995004400050002x

Xing XL, Li TL, Fu YK (2016) Determination of the related strength parameters of unsaturated loess with conventional triaxial test. *Environmental Earth Sciences* 75:82, DOI: 10.1007/s12665-015-4797-5

Xing YC, Gao DH, Jin SL, Zhang AJ, Guo MX (2019) Study on mechanical behaviors of unsaturated loess in terms of moistening

level. *KSCE Journal of Civil Engineering* 23(3):1055-1063, DOI: 10.1007/s12205-019-0848-x

Yin JH, Cheng CM, Kumruzzaman M, Zhou WH (2010) New mixed boundary, true triaxial loading device for testing three-dimensional stress-strain-strength behavior of geomaterials. *Canadian Geotechnical Journal* 47(1):1-15, DOI: 10.1139/T09-075

Zárate MA (2013) Loess records | South America. *Encyclopedia of Quaternary Science* 629-641, DOI: 10.1016/B978-0-444-53643-3.00160-6

Zhang Y, Hu ZQ, Chen H, Xue T (2018) Experimental investigation of the behavior of collapsible loess treated with the acid-addition pre-soaking method. *KSCE Journal of Civil Engineering* 22(11):4373-4384, DOI: 10.1007/s12205-017-0170-4